Available online at www.sciencedirect.com

ScienceDirect

IFAC PapersOnLine 56-2 (2023) 4074–4081

Practical Deployment of Spectral Submanifold Reduction for Optimal Control of High-Dimensional Systems

John Irvin Alora * **Mattia Cenedese** ** **Edward Schmerling** *
George Haller ** **Marco Pavone** *

* *Department of Aeronautics and Astronautics, Stanford University*
(e-mail: {jjalora, schmrlng, pavone}@stanford.edu).
** *Institute for Mechanical Systems, ETH Zürich*
(e-mail: {mattiac, georgehaller}@ethz.ch).

Abstract: Real-time optimal control of high-dimensional, nonlinear systems remains a challenging task due to the computational intractability of their models. While several model-reduction and learning-based approaches for constructing low-dimensional surrogates of the original system have been proposed in the literature, these approaches suffer from fundamental issues which limit their application in real-world scenarios. Namely, they typically lack generalizability to different control tasks, ability to trade dimensionality for accuracy, and ability to preserve the structure of the dynamics. Recently, we proposed to extract low-dimensional dynamics on Spectral Submanifolds (SSMs) to overcome these issues and validated our approach in a highly accurate simulation environment. In this manuscript, we extend our framework to a real-world setting by employing time-delay embeddings to embed SSMs in an observable space of appropriate dimension. This allows us to learn highly accurate, low-dimensional dynamics purely from observational data. We show that these innovations extend Spectral Submanifold Reduction (SSMR) to real-world applications and showcase the effectiveness of SSMR on a soft robotic system.

Keywords: Machine learning in modelling, prediction, control and automation; physics-based modeling for control; nonlinear optimal control; nonlinear system identification

1. INTRODUCTION

The class of systems considered for control is becoming more complex and diverse, to include infinite-dimensional systems (*i.e.,* dynamically-evolving continua) such as those involving fluid flows, deformable or flexible structures, and chemical processes. Controlling these types of systems accurately is challenging because it requires high-dimensional models. Physics-based models of infinite-dimensional systems are governed by partial differential equations, which, after discretization, result in finite, but extremely high-dimensional systems of ordinary differential equations (ODE). Since these ODEs have thousands to millions of dimensions, they are quite computationally intensive to propagate. Therefore, the application of robust optimal control schemes, such as model predictive control (MPC), for real-time control using these models is unrealistic.

In this work, we learn the reduced dynamics of high-dimensional systems on low-dimensional, attracting invariant manifolds called Spectral Submanifolds (SSMs). This *Spectral Submanifold Reduction* (SSMR), yields accurate, very low-dimensional models to be used in real-time optimal control schemes. By learning dynamics on these generic structures, our approach overcomes common drawbacks associated with learning-based techniques. These include lack of generalizability to different control tasks, inability to tractably trade off dimensionality for accuracy, and inability to preserve the structure of the dynamics (Alora et al. (2022)).

Statement of Contributions: Our contributions are two-fold. In this exposition, we

(i) Provide a more comprehensive description of our SSMR approach relative to that given by Alora et al. (2022). Specifically, we detail the theoretical underpinnings of our control-parameterized SSM approach. This allows us to interpret the trajectory of our system under control inputs as living on a time-varying manifold.

(ii) We validate the efficacy of our SSMR framework (which was initially shown in a simulation environment) in the real-world by (a) learning reduced models purely from experimental data using time-delay embeddings and (b) learning a second set of mappings which allow us to extract models based on generic observables for state estimation and control.

We demonstrate that SSMR is competitive *vis-á-viz* the state-of-the-art for the control of a real-world soft robot.

⋆ J.A. is supported by the Secretary of the Air Force STEM Ph.D. Fellowship. This work was supported by the NASA University Leadership Initiative (grant #80NSSC20M0163) and KACST; this article solely reflects the opinions and conclusions of its authors and not any Air Force, NASA, nor KACST entity.

10.1016/j.ifacol.2023.10.1734

Related Work: The prevailing model-based approach in the literature for control of high-dimensional, *linear* dynamical systems leverages projection-based methods as a means for model reduction (Lorenzetti et al. (2021); Ghiglieri and Ulbrich (2014); Alla and Volkwein (2015); Altmüller (2014)) These approaches involve a data-driven procedure to identify linear subspaces which best explain the behavior of the system. The high-dimensional governing equations are then projected down to such a linear subspace, giving a reduced-order model (ROM) of the system for computationally tractable control. While these approaches work well for linear systems, the ROM validity deteriorates rapidly far away from the linearization point.

Various schemes to approximate the nonlinearities for control have been proposed including a piecewise-affine approximation (Tonkens et al. (2021)) and nonlinear balanced truncation (Huang and Kramer (2020)). Unfortunately, these existing approaches still result in relatively high-dimensional models for control (*i.e.,* greater than 20 dimensions). Additionally, the dimension of the ROM can grow rapidly with only a small improvement in accuracy. In this work, we extract ROMs from invariant manifolds which capture the nonlinearities of the system. By identifying the reduced dynamics on these generic structures, we obtain highly accurate, low-dimensional models amenable to real-time control. We do this in a purely data-driven fashion, allowing us to forego the encumbering and code-intrusive process of extracting governing equations from finite element code.

On the other end of the literature spectrum, data-driven approaches using neural networks (NN) have been used to learn low-dimensional dynamics from observed transitions of the system (Thuruthel et al. (2018); Greydanus et al. (2019); Cranmer et al. (2020)). The underlying assumption behind these approaches is that there exists low-dimensional, latent dynamics that one can learn, which explain the observations. This idea is similar to the setting in this work, but rather than infer the existence of these dynamics, we explicitly target structures which we know exist in the phase space of dissipative, physical systems. While the existing approaches rarely preserve the properties of the underlying dynamics, our strategy allows us to encode these properties directly. We tailor our learning approach to best capture this structure and the reduced dynamics on it.

A popular data-driven approach which has garnered significant interest within the controls community is based on the Koopman operator (Mezić (2005)). This approach involves finding a nonlinear change of coordinates which approximately transforms the original nonlinear system into a linear system. Koopman operator-based approaches are thus amenable to established linear control schemes and approximation of the Koopman operator has been used in a variety of control applications (Bruder et al. (2019b,a)). While conceptually appealing, most physical systems do not admit exact finite-dimensional, linear representations. Additionally, attempts to accurately approximate complex physical systems require a larger set of observable basis functions, which leads to numerical conditioning issues of the approximate Koopman operator, as shown by Dahdah and Forbes (2022). Lastly, similar to the other data-driven approaches, Koopman operator-based approaches rarely preserve the structure of the dynamics, as shown in Alora et al. (2022). By explicitly targeting rigorous and generic structures in the high-dimensional system's phase space, we are able to extract ROMs which overcome these limitations.

Organization: In Section 2 we describe the class of high-dimensional systems we consider for control and pose the associated nonlinear optimal control problem. In Section 3 we summarize recent results on SSMs, justify the construction of control-parameterized SSMs, and derive the form of the parameterizations and reduced dynamics with control. In Section 4 we detail the learning procedure to extract these mappings from data and then formulate the reduced order optimal control problem. We present our hardware results with discussion in Section 5.

2. PROBLEM FORMULATION

2.1 Notation

The set of integers and reals are denoted by $\mathbb{Z}$ and $\mathbb{R}$, with their non-negative subsets denoted by $\mathbb{N}$ and $\mathbb{R}_+$. The complex numbers are denoted by $\mathbb{C}$. $\mathbb{T}^\ell = \mathbb{R}^\ell / \left(2\pi\mathbb{Z}^\ell\right)$ represents the ℓ-dimensional torus. C^k represents the space of k-times continuously differentiable functions and C^a represents the space of analytic functions. $L^2(V, W)$ is the space of square integrable functions from a complete vector space V to W. $\mathcal{O}(\cdot)$ represents Landau big-O notation.

2.2 High-Dimensional Optimal Control Problem

We consider control-affine systems with $\mathcal{N} \in \mathbb{N}$ degrees of freedom (DOF). Such systems can be written in first-order form with state vector $\mathbf{x}^f(t) \in \mathbb{R}^{n_f}$ (where f denotes *full* state, as opposed to the *reduced* state $\mathbf{x}$ introduced in Theorem 8, Section 3.1) as

$$\dot{\mathbf{x}}^f(t) = \mathbf{A}\mathbf{x}^f(t) + \mathbf{f}_{\mathrm{nl}}(\mathbf{x}^f(t)) + \varepsilon\mathbf{B}\mathbf{u}(t), \tag{1}$$

where $n_f = 2\mathcal{N}$, $\mathbf{A} \in \mathbb{R}^{n_f \times n_f}$, $\mathbf{B} \in \mathbb{R}^{n_f \times m}$ represents the linear control matrix, and $\mathbf{f}_{\mathrm{nl}} : \mathbb{R}^{n_f} \to \mathbb{R}^{n_f}$ represents the nonlinearities in the dynamics. For mechanical systems, this can represent high-dimensional finite-element models (FEM), where $\mathcal{N}$ represents the number of nodes in the mesh, which converge to the exact model of control-affine systems in the continuum limit (*i.e.,* $\mathcal{N} \to \infty$) (Della Santina et al. (2021)). In this work, we consider control tasks near the vicinity of the system's equilibrium point, thus ε satisfies the following condition

Assumption 1. The magnitude of the control inputs should be small compared to the autonomous dynamics *i.e.,* the parameter ε satisfies $0 < \varepsilon \ll 1$.

This means that the control effort is moderate, *i.e.,* the control term does not dominate the right hand side in Equation (1). Since our approach relies on estimating dynamics on smooth, attracting manifolds attached to an equilibrium point, we introduce the following assumptions on the form of $\mathbf{A}$ and $\mathbf{f}_{\mathrm{nl}}$.

Assumption 2. $\mathbf{A}$ is Hurwitz-stable, *i.e.,* every eigenvalue of $\mathbf{A}$ has negative real part. Thus, the origin is an asymptotically stable fixed point for $\varepsilon = 0$.

Assumption 3. $\mathbf{f}_{\mathrm{nl}} \in C^a$ belongs to the class of analytic functions and satisfies $\mathbf{f}_{\mathrm{nl}}(\mathbf{0}) = \mathbf{0}$, $\partial\mathbf{f}_{\mathrm{nl}}(\mathbf{0})/\partial\mathbf{x}^f = \mathbf{0}$.

Assumption 2 is generically satisfied by many physical systems such as robotic arms conducting pick and place tasks in a constrained workspace. Additionally, systems which exhibit smooth behavior satisfy Assumption 3. Our approach can also handle systems with mild discontinuities such that these behaviors can be approximated smoothly, as shown by Cenedese et al. (2022b). As we develop SSMR theory, we will make several more assumptions after developing notation. We claim that these assumptions are generically satisfied for a large class of physical systems, such as continuum robots.

We now pose the problem of controlling Equation (1) to follow arbitrary and dynamic trajectories in the vicinity of the origin. Consider the following continuous-time, optimal control problem (OCP) with quadratic cost and polytopic constraints in states and control:

$$\begin{aligned} \underset{\mathbf{u}(\cdot)}{\text{minimize}} \quad & \|\delta\mathbf{z}(t_f)\|^2_{\mathbf{Q}_\text{f}} + \int_{t_0}^{t_f} \Big(\|\delta\mathbf{z}(t)\|^2_{\mathbf{Q}} + \|\mathbf{u}(t)\|^2_{\mathbf{R}} \Big) dt, \\ \text{subject to} \quad & \dot{\mathbf{x}}^f(t) = \mathbf{A}\mathbf{x}^f(t) + \mathbf{f}_\text{nl}(\mathbf{x}^f(t)) + \mathbf{B}\mathbf{u}(t), \qquad (2) \\ & \mathbf{y}(t) = \mathbf{h}(\mathbf{x}^f(t)), \quad \mathbf{z}(t) = \mathbf{C}\mathbf{y}(t), \\ & \mathbf{u} \in \mathcal{U}, \quad \mathbf{z} \in \mathcal{Z}. \end{aligned}$$

Here, $\delta\mathbf{z}(t) = \mathbf{z}(t) - \bar{\mathbf{z}}(t)$ is the tracking difference between the performance variable, $\mathbf{z}(t) \in \mathbb{R}^o$ and the desired trajectory $\bar{\mathbf{z}}(t) \in \mathbb{R}^o$. The observed state is denoted as $\mathbf{y}(t) \in \mathbb{R}^p$ and $[t_0, t_f]$ represents the time horizon. $\mathbf{Q}, \mathbf{Q}_\text{f} \in \mathbb{R}^{o\times o}$ are positive semi-definite matrices which represent the stage and terminal costs, respectively, over the performance variables, while $\mathbf{R}$ is a positive-definite matrix representing the cost on controls. The constraint sets are defined as $\mathcal{U} := \{\mathbf{u}(t) \in \mathbb{R}^m : \mathbf{M}_\text{u}\mathbf{u}(t) \leq \mathbf{b}_\text{u}\}$ and $\mathcal{Z} := \{\mathbf{z} \in \mathbb{R}^o : \mathbf{M}_\text{z}\mathbf{z}(t) \leq \mathbf{b}_\text{z}\}$ with $\mathbf{M}_\text{u} \in \mathbb{R}^{n_u\times m}$ and $\mathbf{M}_\text{z} \in \mathbb{R}^{n_z\times o}$, where n_u and n_z represent the number of constraints in the inputs and the observed states, respectively. Lastly, $\mathbf{C} \in \mathbb{R}^{o\times p}$ is a selection matrix of states that we observe, while the functions $\mathbf{g} : \mathbb{R}^o \to \mathbb{R}^{n_f}$ and $\mathbf{h} : \mathbb{R}^{n_f} \to \mathbb{R}^p$ map the performance variable to the full state and the full state to the observed state, respectively. We also make following assumption:

Assumption 4. $\mathbf{g}, \mathbf{h} \in C^a$ also belong to the class of analytic functions and satisfies $\mathbf{g}(0) = \mathbf{h}(0) = 0$.

In most settings, our observables are a subset of the nodes of our system or are related by a combination of rotations and translations. Hence, for a myriad of applications, Assumption 4 is generically satisfied.

For high-dimensional dynamical systems, *i.e.,* $n_f \gg 1$, dimensionality of Equation (1) makes it intractable to solve the OCP (2) in real-time. Thus, we seek a low-dimensional approximation of Equation (1) that enables online control and allows us to approximate a solution to the OCP.

3. CONTROL DYNAMICS ON LOW-DIMENSIONAL INVARIANT MANIFOLDS

3.1 Summary of Spectral Submanifolds

We define an n-dimensional spectral subspace E as the direct sum of an arbitrary collection of n eigenspaces of $\mathbf{A}$,

$$E := E_{j_1} \oplus E_{j_2} \oplus ... \oplus E_{j_n},$$

where E_{j_k} denotes the real eigenspace corresponding to an eigenvalue λ_{j_k} of $\mathbf{A}$. Let Λ_E be the set of eigenvalues related to E and Λ_out be that of eigenvalues not related to E. If $\min_{\lambda\in\Lambda_E} \text{Re}(\lambda) > \max_{\lambda\in\Lambda_\text{out}} \text{Re}(\lambda)$, then E represents the slowest spectral subspace of order n. Intuitively, the slowest spectral subspace corresponds to the dominant modes representing the persisting dynamics of the system.

Recent results in nonlinear dynamics establish the existence of unique, smoothest invariant structures in the phase space of Equation (1), Haller and Ponsioen (2016). SSMs are nonlinear continuations of the spectral subspaces of the linearization of (1). The SSM corresponding to E in the autonomous part of (1) is defined as follows.

Definition 5. An autonomous SSM $\mathcal{W}(E)$, corresponding to a spectral subspace E of the operator $\mathbf{A}$ is an invariant manifold of the autonomous part $\dot{\mathbf{x}}^f_\text{aut}(t) = \mathbf{A}\mathbf{x}^f_\text{aut}(t) + \mathbf{f}_\text{nl}(\mathbf{x}^f_\text{aut}(t))$ of the nonlinear system (1), *i.e.,*

$$\mathbf{x}^f_\text{aut}(0) \in \mathcal{W}(E) \implies \mathbf{x}^f_\text{aut}(t) \in \mathcal{W}(E), \quad \forall t \in \mathbb{R},$$

such that,

(1) $\mathcal{W}(E)$ is tangent to E at the origin and has the same dimension as E,
(2) $\mathcal{W}(E)$ is strictly smoother than any other invariant manifold satisfying condition 1 above.

A slow SSM is associated with a spectral subspace containing the slowest decaying eigenvectors of the linearized system. SSMs as described in Definition 5 turn out to exist as long as the following assumption is satisfied

Assumption 6. The spectrum Λ_E, has no low-order resonance relationship with any eigenvalue in the outer spectrum Λ_out (see Haller and Ponsioen (2016); Cenedese et al. (2022a) for details).

In the non-autonomous setting of quasi-periodic forcing, SSMs are envisioned similarly to the autonomous setting and the role of the fixed point is taken over by the quasi-periodic orbit γ_ε created by the small-amplitude control force. A nonautonomous, time-varying SSM $\mathcal{W}(E, \gamma_\varepsilon)$ is then a fibre bundle that perturbs smoothly from the vector bundle $\gamma_\varepsilon \times E$ under the addition of control $\mathbf{u}(t) = \mathbf{f}_\text{ext}(\mathbf{x}^f, \mathbf{\Omega}t)$, where $\mathbf{\Omega} = (\boldsymbol{\omega}_1, \ldots, \boldsymbol{\omega}_\ell)$ is the incommensurable frequency basis of $\mathbf{f}_\text{ext} \in L^2$.

Definition 7. A quasi-periodic SSM $\mathcal{W}(E, \gamma_\varepsilon)$, corresponding to a spectral subspace E of the operator $\mathbf{A}$ is an invariant manifold of the nonlinear system (1), under quasi-periodic $\mathbf{u}(t) = \mathbf{f}_\text{ext}(\mathbf{x}^f, \mathbf{\Omega}t)$ such that

(1) $\mathcal{W}(E, \gamma_\varepsilon)$ is a subbundle of the normal bundle $N\gamma_\varepsilon$ of the periodic orbit γ_ε, satisfying $\dim \mathcal{W}(E, \gamma_\varepsilon) = \dim E + 1$,
(2) $\mathcal{W}(E)$ perturbs smoothly from the spectral subspace E of the linearized system under the addition of nonlinear and control terms in Equation 1.
(3) $\mathcal{W}(E, \gamma_\varepsilon)$ has strictly more continuous derivatives along γ_ε than any other invariant manifold satisfying conditions 1 and 2 above.

Additionally, by Assumption 1, the following theorem guarantees the existence of the time-varying SSM.

Theorem 8. Consider a spectral subspace E with $\dim E = n$ and its associated eigenvalues (counting multiplicities) listed as $\lambda_1, \ldots, \lambda_n$. Suppose Assumptions (2), (3), and (6) are satisfied.

Then the following holds:

(1) There exists a time-varying, quasi-periodic SSM, $\mathcal{W}(E, \gamma_\varepsilon)$ for system (1) that depends smoothly on the parameter ε and is unique in the class of $C^{\Sigma(E)+1}$ invariant manifolds, where $\Sigma(E)$ represent the absolute spectral quotient as defined in Haller and Ponsioen (2016).

(2) $\mathcal{W}(E, \gamma_\varepsilon)$ can be viewed as an embedding of an open set $\mathcal{V}$ into the state space of System (1) via the map

$$\mathbf{W}_\varepsilon(\mathbf{x}, \boldsymbol{\Omega}t) : \mathcal{V} \subset \mathbb{R}^n \times \mathbb{T}^\ell \to \mathbb{R}^{n_f}, \tag{3}$$

with the quasi-periodic frequency $\boldsymbol{\Omega} \in \mathbb{T}^\ell$ and reduced state, $\mathbf{x} \in \mathbb{R}^n$.

(3) There exists a polynomial function with respect to $\mathbf{x}$, $\mathbf{R}_\varepsilon(\mathbf{x}, \boldsymbol{\varphi}) : \mathcal{V} \to \mathbb{R}^n$ satisfying the invariance equation

$$\begin{aligned}\mathbf{A}\mathbf{W}_\varepsilon(\mathbf{x}, \boldsymbol{\varphi}) + \mathbf{f}_{\mathrm{nl}}(\mathbf{W}_\varepsilon(\mathbf{x}, \boldsymbol{\varphi})) + \varepsilon \mathbf{B}\mathbf{f}_{\mathrm{ext}}(\mathbf{W}_\varepsilon(\mathbf{x}, \boldsymbol{\varphi}), \boldsymbol{\varphi}) \\ = \mathrm{D}_{\mathbf{x}}\mathbf{W}_\varepsilon(\mathbf{x}, \boldsymbol{\varphi})\mathbf{R}_\varepsilon(\mathbf{x}, \boldsymbol{\varphi}) + \frac{d}{dt}\mathbf{W}_\varepsilon(\mathbf{x}, \boldsymbol{\varphi}),\end{aligned} \tag{4}$$

where $\boldsymbol{\varphi} = \boldsymbol{\Omega}t$, such that the reduced dynamics on the SSM is given by

$$\dot{\mathbf{x}} = \mathbf{R}_\varepsilon(\mathbf{x}, \boldsymbol{\varphi}). \tag{5}$$

Proof. This is a restatement of Theorem 4 in Haller and Ponsioen (2016) in our setting, which is deduced from the abstract results on whiskers of invariant tori in Haro and de la Llave (2006).

For general control inputs where $\mathbf{u}(t)$ is no longer necessarily quasi-periodic, the trajectory of System (5) will remain close to the full state trajectory. To make this intuition formal, let us define the following control-parameterized mappings

Definition 9. Define $\mathbf{W} : \mathbb{R}^n \times \mathcal{U} \to \mathbb{R}^{n_f}$ and $\mathbf{R} : \mathbb{R}^n \times \mathcal{U} \to \mathbb{R}^n$ as control-parameterized mappings whose autonomous parts (*i.e.,* the terms which depend only on $\mathbf{x}$) are equal to $\mathbf{W}_\varepsilon$ and $\mathbf{R}_\varepsilon$, respectively.

In the following corollary, we show that it is possible to interpret the trajectory of the system under $\mathbf{u}(t)$ as lying approximately on a time-varying, invariant manifold $\mathcal{W}(E, \gamma_\varepsilon)$.

Corollary 10. Suppose $\mathbf{u}(t)$ is bounded and smooth, *i.e.,* $\|\mathbf{u}(t)\| \leq M$, $\forall t \in \mathbb{R}_+$ and $\mathbf{u} \in L^2$. Then the following holds,

(1) $\mathbf{W}(\mathbf{x}, \mathbf{u})$ and $\mathbf{R}(\mathbf{x}, \mathbf{u})$ can be arbitrarily approximated by a parameterization $\mathbf{W}_\varepsilon(\mathbf{x}, \boldsymbol{\Omega}t)$ and $\mathbf{R}_\varepsilon(\mathbf{x}, \boldsymbol{\Omega}t)$ for some $\boldsymbol{\Omega} \in \mathbb{T}^\ell$ over a finite time-interval $t \in [0, T]$ with $T \in \mathbb{R}_+$.

(2) Furthermore, there exists a polynomial with respect to $\mathbf{x}$ such that the following relationship holds

$$\begin{aligned}\mathbf{A}\mathbf{W}(\mathbf{x}, \mathbf{u}) + \mathbf{f}_{\mathrm{nl}}(\mathbf{W}(\mathbf{x}, \mathbf{u})) + \varepsilon \mathbf{B}\mathbf{u} \\ = \mathrm{D}_{\mathbf{x}}\mathbf{W}(\mathbf{x}, \mathbf{u})\mathbf{R}(\mathbf{x}, \mathbf{u}) + \frac{d}{dt}\mathbf{W}(\mathbf{x}, \mathbf{u})\end{aligned} \tag{6}$$

Proof. Define a periodic function with respect to $\mathbf{u}$ over a finite time interval T as $\mathbf{g}_\epsilon(t) := \mathbf{u}(t)\mathbb{1}_{0 \leq t < T - \frac{\epsilon}{8M^2}}(t) + \mathbf{u}(0)\mathbb{1}_{T - \frac{\epsilon}{8M^2} \leq t < T}(t)$, where $\mathbb{1}_{(\cdot)}$ denotes the standard indicator function. We first show that $\mathbf{u}(t)$ can be arbitrarily approximated by $\mathbf{g}_\epsilon(t)$:

$$\begin{aligned}&\int_0^T ||\mathbf{g}_\epsilon(t) - \mathbf{u}(t)||^2 dt \\ &= \int_0^{T - \frac{\epsilon}{8M^2}} ||\mathbf{g}_\epsilon(t) - \mathbf{u}(t)||^2 dt + \int_{T - \frac{\epsilon}{8M^2}}^T ||\mathbf{g}_\epsilon(t) - \mathbf{u}(t)||^2 dt \\ &= \int_{T - \frac{\epsilon}{8M^2}}^T ||\mathbf{g}(0) - \mathbf{u}(t)||^2 dt < \int_{T - \frac{\epsilon}{8M^2}}^T 4M^2 dt = \frac{\epsilon}{2}.\end{aligned}$$

By Theorem 1 of Samoilenko and Teplinsky (2013), the set of values of some quasi-periodic function $\mathbf{u}_\epsilon(\boldsymbol{\Omega}t) = \mathbf{f}_{\mathrm{ext}}(\mathbf{x}^f, \boldsymbol{\Omega}t)$ is dense in the set of values of $\mathbf{g}_\epsilon(t)$ *i.e.,* $||\mathbf{u}_\epsilon(\boldsymbol{\Omega}t) - \mathbf{g}_\epsilon(t)||^2 \leq \frac{\epsilon}{2T}$. Thus,

$$\begin{aligned}&\int_0^T ||\mathbf{u}_\epsilon(\boldsymbol{\Omega}t) - \mathbf{u}(t)||^2 dt \\ &\leq \int_0^T \Big(||\mathbf{u}_\epsilon(\boldsymbol{\Omega}t) - \mathbf{g}_\epsilon(t)||^2 + ||\mathbf{g}_\epsilon(\boldsymbol{\Omega}t) - \mathbf{u}(t)||^2\Big) dt < \epsilon.\end{aligned}$$

Since the autonomous parts of $\mathbf{W}$ and $\mathbf{R}$ equal those of $\mathbf{W}_\varepsilon$ and $\mathbf{R}_\varepsilon$, respectively, then by the approximation argument above, there exists $\boldsymbol{\Omega} \in \mathbb{T}^\ell$ such that $\mathbf{W}_\varepsilon(\mathbf{x}, \boldsymbol{\Omega}t)$ and $\mathbf{R}_\varepsilon(\mathbf{x}, \boldsymbol{\Omega}t)$ approximate $\mathbf{W}$ and $\mathbf{R}$, respectively over finite T. This proves part (1). Part (2) follows from part (1) and Theorem 8, resulting in a control-dependent SSM parameterization $\mathbf{W}(\mathbf{x}, \mathbf{u})$ and $\mathbf{R}(\mathbf{x}, \mathbf{u})$ which satisfies Equation (6), at least for finite time. □

Theorem 8 and Corollary 10 convey the fact that SSMs are ideal candidates for model reduction because they exponentially attract nearby trajectories. In the following section, we exploit the low-dimensional structures offered by SSMs to extract reduced-order, control dynamics by learning $\mathbf{W}$ and $\mathbf{R}$.

3.2 Low-Dimensional Models on SSMs

In practice, we do not have access to the full state $\mathbf{x}^f$. Though, by Whitney's embedding theorem, we can embed the SSM and reduced dynamics in a space consisting of observables, $\mathbf{y} \in \mathbb{R}^p$ where $p \geq 2n+1$. If $\mathbf{y}$ does not satisfy this condition, then we can invoke Taken's embedding theorem and use time-delay embeddings of $\mathbf{y}$ (Kim et al. (1999)), such that our new observed measurements include current and past measurements, to embed $\mathcal{W}(E, \gamma_\varepsilon)$ in a space with sufficient dimension. Thus, our SSM parameterizations in the observed space, using the graph-style approach of Cenedese et al. (2022a), is

$$\begin{aligned}\mathbf{x} &= \mathbf{V}_0^\top \mathbf{y}, \\ \mathbf{y} &= \mathbf{V}_0 \mathbf{x} + \mathbf{w}_{\mathrm{nl}}(\mathbf{x}) + \varepsilon \mathbf{w}_{\mathbf{u}}(t), \\ \dot{\mathbf{x}} &= \mathbf{R}_0 \mathbf{x} + \mathbf{r}_{\mathrm{nl}}(\mathbf{x}) + \varepsilon \mathbf{r}_{\mathbf{u}}(t),\end{aligned} \tag{7}$$

where the columns of $\mathbf{V}_0 \in \mathbb{R}^{p \times n}$ span the tangent space of $\mathcal{W}(E, \gamma_\varepsilon)$ and the two maps $\mathbf{w}_{\mathrm{nl}} : \mathbb{R}^n \to \mathbb{R}^p$ and $\mathbf{r}_{\mathrm{nl}} : \mathbb{R}^n \to \mathbb{R}^n$ represent the nonlinear terms in the SSM parameterization and reduced dynamics, respectively. The maps $\mathbf{w}_{\mathbf{u}} : \mathbb{R}_+ \to \mathbb{R}^p$ and $\mathbf{r}_{\mathbf{u}} : \mathbb{R}_+ \to \mathbb{R}^n$ represent the control-parameterized terms for some fixed $\mathbf{u}$.

Under the additional assumption

Assumption 11. The outer modes have negligible effects in the $\mathcal{O}(\varepsilon)$-correction of the non-autonomous SSM geometry.

One can show using the invariance properties of the SSM, that

$$\begin{aligned}\mathbf{w}_{\mathbf{u}}(t) &= \mathbf{w}_{\mathbf{u}}(0) + \mathbf{B}_{\mathbf{w}} \int_0^t \mathbf{u}(s) ds, \\ \mathbf{r}_{\mathbf{u}}(t) &= \mathbf{B}_{\mathbf{r}} \mathbf{u}(t),\end{aligned} \tag{8}$$

where $\mathbf{B}_{\mathbf{r}} \in \mathbb{R}^{o \times m}$ is the control matrix describing how the input influences the reduced dynamics while $\mathbf{B}_{\mathbf{w}} \in \mathbb{R}^{n \times m}$ describes how the SSM is translated in the phase space. Assumption 11 is generically satisfied in slow SSMs of mechanical systems where the outer modes are much stiffer than those related to the SSM (Jain and Haller (2021)), as in the example we discuss later.

In many control settings, it might be preferable to use a different set of observables that differ from those used to construct the SSM. We find that good closed-loop performance necessitates working with models that do not involve time-delays. Thus, while we retain the reduced dynamics in Equation (7) regressed from possibly time-delayed observations, we now seek mappings that relate our reduced coordinates to our new observables. Without loss of generality, suppose our desired observables for control are the performance variables, $\mathbf{z}$. By Assumption (4), *i.e.,* smoothness of our observable functions, we can relate our reduced coordinates with the new observables via a new coordinate chart and parameterization through the nonlinear mappings

$$\begin{aligned}\mathbf{x} &= \mathbf{v}_z(\mathbf{z}), \\ \mathbf{z} &= \mathbf{w}_z(\mathbf{x}, \mathbf{u}) = \mathbf{w}_a(\mathbf{x}) + \varepsilon \mathbf{w}_{\mathbf{u},z}(t).\end{aligned} \tag{9}$$

where $\mathbf{w}_z : \mathbb{R}^o \to \mathbb{R}^n$ and $\mathbf{v}_z : \mathbb{R}^{n \times m} \to \mathbb{R}^o$ are the reduced coordinate and observable parameterizations on the SSM, respectively, $\mathbf{w}_a : \mathbb{R}^n \to \mathbb{R}^o$ is the autonomous part of $\mathbf{w}_z$, and $\mathbf{w}_{\mathbf{u},z}(t) = \mathbf{w}_{1,z}(0) + \mathbf{B}_{\mathbf{w},z} \int_0^t \mathbf{u}(s) ds$ is similar to $\mathbf{w}_{\mathbf{u}}(t)$, but is now a mapping with respect to $\mathbf{z}$. In the following section, we seek to learn the reduced dynamics in (7,8) and the paramaterizations in (9) by approximating the mappings that describe the trajectory of our observed states on SSMs.

4. LEARNING LOW-DIMENSIONAL DYNAMICS ON INVARIANT MANIFOLDS

Our three-step SSMR procedure involves: (1) collecting trajectories at or near the SSM. (2) learning the SSM geometry and the reduced dynamics in (7), followed by (3) learning the linear control matrices that describes the effect of the controls in the reduced coordinates.

4.1 Learning Autonomous Dynamics

To describe the autonomous part of the geometry and reduced dynamics on $\mathcal{W}(E, \gamma_\varepsilon)$, we express the mappings $\mathbf{v}_z$ and $\mathbf{w}_a$ via a Taylor series expansion

$$\begin{aligned}\mathbf{x} &= \mathbf{v}_z(\mathbf{z}) = \tilde{\mathbf{V}}_0 \mathbf{z} + \tilde{\mathbf{V}} \mathbf{z}^{2:n_v} \\ \mathbf{z}_a &= \mathbf{w}_a(\mathbf{x}) = \mathbf{W}_0 \mathbf{x} + \mathbf{W} \mathbf{x}^{2:n_w} \\ \dot{\mathbf{x}}_a &= \mathbf{r}_a(\mathbf{x}) = \mathbf{R}_0 \mathbf{x} + \mathbf{R} \mathbf{x}^{2:n_r}\end{aligned} \tag{10}$$

where $\mathbf{x}^{2:n_v}$ is the family of all monomials from order 2 to n_v, and $n_v, n_w, n_r \in \mathbb{R}_+$ are the desired order of the Taylor series expansion for approximating the maps of the SSM. To learn the autonomous parts of the geometry and reduced dynamics in Equation (7), the training data should involve only trajectories that are near the SSM. Thus, we obtain training data snapshots by initializing the system along various points in its configuration space, then collect the observed state trajectory as it decays to its equilibrium point. Since we aim to infer the geometry of our SSM from data, our decaying trajectories should be as close to the SSM as possible. Hence, each decay trajectory is truncated to remove initial transients converging to the SSM. We denote the truncated training dataset of decaying trajectories as $\mathcal{D}_a$.

We first approximate the basis for the tangent space to which we attach our SSM by finding the n dominant modes of Equation (1) (*i.e.,* the n columns of $\mathbf{V}_0$). To do this we carry out singular value decomposition (SVD) on our dataset $\mathcal{D}_a$ and pick the n leading directions that capture a majority of the variance in the data. Indeed, for systems that do not feature strong nonlinearities, SVD is able to obtain a close estimate for the spectral subspace E to which the SSM is tangent as shown in Axås et al. (2022). Thus, we make the following assumption

Assumption 12. SVD of the leading n modes on the dataset $\mathcal{D}_a$ can capture the tangent space of the SSM, spanned by the columns of $\mathbf{V}_0$.

Under Assumption (12), we then form the set of reduced coordinates $\{\mathbf{x} : \mathbf{x} = \mathbf{V}_0^\top \mathbf{y}\}$ from our training trajectories $\mathbf{y} \in \mathcal{D}_a$. With slight abuse of notation, we denote $(\mathbf{x}, \mathbf{y}, \mathbf{z}) \in \mathcal{D}_a$ to specify data either obtained or inferred from autonomous trajectories. Here $\mathbf{z}$ may be a subset of the observables $\mathbf{y}$ or obtained after post-processing $\mathbf{y}$. We can then find the unknown coefficients in Equation (10) via polynomial regression

$$\begin{aligned}(\tilde{\mathbf{V}}_0^*, \tilde{\mathbf{V}}^*) &= \underset{\tilde{\mathbf{V}}_0, \tilde{\mathbf{V}}^*}{\arg\min} \sum_{(\mathbf{x},\mathbf{z}) \in \mathcal{D}_a} \left\| \mathbf{x} - \tilde{\mathbf{V}}_0 \mathbf{z} - \tilde{\mathbf{V}} \mathbf{z}^{2:n_v} \right\|_2^2, \\ (\mathbf{W}_0^*, \mathbf{W}^*) &= \underset{\mathbf{W}_0, \mathbf{W}^*}{\arg\min} \sum_{(\mathbf{x},\mathbf{z}) \in \mathcal{D}_a} \left\| \mathbf{z} - \mathbf{W}_0 \mathbf{x} - \mathbf{W} \mathbf{x}^{2:n_v} \right\|_2^2, \\ (\mathbf{R}_0^*, \mathbf{R}^*) &= \underset{\mathbf{R}_0, \mathbf{R}^*}{\arg\min} \sum_{\mathbf{x} \in \mathcal{D}_a} \left\| \dot{\mathbf{x}} - \mathbf{R}_0 \mathbf{x} - \mathbf{R} \mathbf{x}^{2:n_r} \right\|_2^2.\end{aligned} \tag{11}$$

The time derivative in (11) can be computed using standard finite difference schemes if the sampling time of $\mathcal{D}_a$ is much smaller than the Nyquist sampling time of the fastest mode in the SSM dynamics.

4.2 Learning Linear Control Dynamics

We set $\varepsilon = 1$, without loss of generality, for the rest of the exposition. Once the autonomous parameterizations in (10) are known, we can regress the control matrices $\mathbf{B}_{\mathbf{r}}$ and $\mathbf{B}_{\mathbf{w},z}$.

To do this, we collect a new dataset $(\mathbf{y}, \mathbf{z}) \in \mathcal{D}_u$ of state transitions obtained from exploring the actuation space of the system. We do this by generating a smooth sequence of inputs, $\mathbf{u}$, *e.g.,* through periodic actuation at various control amplitudes and recording the corresponding (possibly time-delayed) observed state trajectories $\mathbf{y}$. We then map $\mathbf{y} \in \mathcal{D}_u$ down to the reduced coordinates $\mathbf{x} = \mathbf{V}_0^\top \mathbf{y}$ and regress the control matrices as follows,

$$\mathbf{B}_\mathbf{r}^* = \arg\min_{\mathbf{B}_\mathbf{r}} \sum_{\mathbf{x}\in\mathcal{D}_u} ||\dot{\mathbf{x}} - \mathbf{R}_0\mathbf{x} - \mathbf{R}\mathbf{x}^{2:n_r} - \mathbf{B}_\mathbf{r}\mathbf{u}||_2^2,$$
$$\mathbf{B}_{\mathbf{w},z}^* = \arg\min_{\mathbf{B}_{\mathbf{w},z}} \sum_{(\mathbf{x},\mathbf{z})\in\mathcal{D}_u} \left\| \frac{d}{dt}(\mathbf{z} - \mathbf{w}_a(\mathbf{x})) - \mathbf{B}_{\mathbf{w},z}\mathbf{u} \right\|_2^2 . \quad (12)$$

These control matrices constrain the effect of the inputs on the shape of the SSM and describes how the inputs translate the SSM in the system's phase space. Thus, the parameterization of the coordinate chart, the parameterization of our time-varying SSM, $\mathbf{W}(\mathbf{x}, \mathbf{u})$, and the controlled reduced dynamics on it are

$$\begin{aligned} \mathbf{x} &= \mathbf{v}_z(\mathbf{z}) = \tilde{\mathbf{V}}_0\mathbf{z} + \tilde{\mathbf{V}}\mathbf{z}^{2:n_v} \\ \mathbf{z} &= \mathbf{w}_z(\mathbf{x}) = \mathbf{W}_0\mathbf{x} + \mathbf{W}\mathbf{x}^{2:n_w} + \mathbf{B}_{\mathbf{w},z}\int_0^t \mathbf{u}(s)ds \quad (13) \\ \dot{\mathbf{x}} &= \mathbf{r}(\mathbf{x}) = \mathbf{R}_0\mathbf{x} + \mathbf{R}\mathbf{x}^{2:n_r} + \mathbf{B}_\mathbf{r}\mathbf{u}. \end{aligned}$$

4.3 Reduced Order Optimal Control Problem

Learning the parameterization of the SSM enables us to learn the intrinsic physics of our system, leading to low-dimensional and accurate reduced models with $n \ll n_f$. This allows us to approximate the OCP in (2) by posing an optimization problem with respect to the dynamics on the SSM as follows

$$\begin{aligned} \underset{\mathbf{u}(\cdot)}{\text{minimize}} \quad & \|\delta\mathbf{z}(t_f)\|_{\mathbf{Q}_f}^2 + \int_{t_0}^{t_f} \Big(\|\delta\mathbf{z}(t)\|_\mathbf{Q}^2 + \|\mathbf{u}(t)\|_\mathbf{R}^2 \Big) dt \\ \text{subject to} \quad & \mathbf{x}(0) = \mathbf{v}_z(\mathbf{z}(0) - \mathbf{z}_{\text{eq}}), \\ & \dot{\mathbf{x}}(t) = \mathbf{r}(\mathbf{x}(t)) + \mathbf{B}_r\mathbf{u}(t), \\ & \mathbf{z}(t) = \mathbf{w}_z(\mathbf{x}(t), \mathbf{u}(t)) + \mathbf{z}_{\text{eq}}, \quad (14) \\ & \mathbf{z}(t) \in \mathcal{Z}, \quad \mathbf{u}(t) \in \mathcal{U}, \end{aligned}$$

where $\mathbf{z}_{\text{eq}} \in \mathbb{R}^o$ is the performance state at equilibrium. To solve the approximate OCP (14) numerically, we discretize the continuous-time system and use Sequential Convex Programming (SCP) to transform (14) into a sequence of quadratic programs. If n is small enough, we can compute the solution to the resulting approximate OCP in real-time.

5. HARDWARE EXPERIMENTS

In this section we demonstrate our proposed SSMR-based control scheme through hardware experiments on the Diamond soft robot in Figure 1. We compare our approach against two state-of-the-art approaches, namely Trajectory-Piecewise Linear (TPWL) (Tonkens et al. (2021)) and a Koopman operator-based approach (Bruder et al. (2019a)).

5.1 Hardware Setup

Our experimental robot platform is equipped with various components for actuation, sensing, and computation. Four Dynamixel XM430-W350-T torque-enabled servos are used to control the tension in the actuation cables. Commands are sent to the servos using the DynamixelSDK Robot Operating System (ROS) library. Next, we use the Motive OptiTrack motion capture system to track the position of the motion capture markers attached to the robot's elbows and end effector (located at its tip), in real-time. We numerically differentiate position in order to get the velocities of each marker. These positions and velocities are transformed into the robot's local reference frame and then streamed as ROS topics.

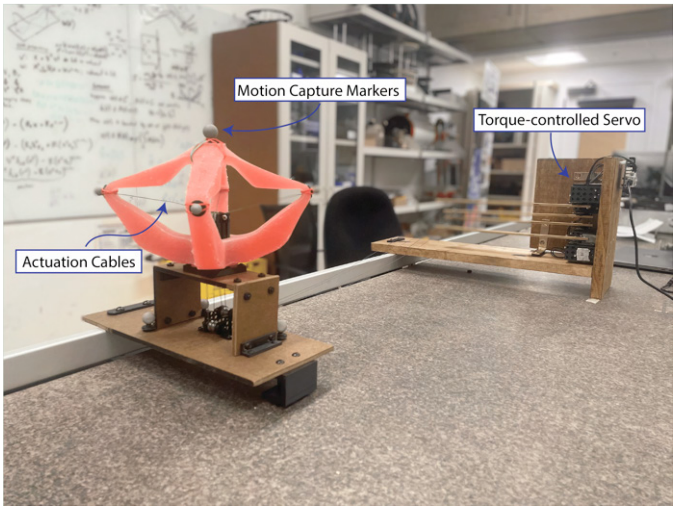

Fig. 1. Hardware platform setup of the elastomer "Diamond" soft robot equipped with motion capture and torque-controlled servos.

Our control scheme is implemented in Python as a ROS package [1] and run on a Lenovo Thinkpad E590 laptop with a 1.6 GHz Intel Core i5 processor and 8 GB of RAM. The optimization problem is setup in CVXPY (Diamond and Boyd (2016); Agrawal et al. (2018)) and solved using Gurobi (Gurobi Optimization, LLC (2022)) and OSQP (Stellato et al. (2020)).

5.2 Model and Controller Parameters

System identification of the TPWL FEM model and calibration of the sensors and actuators were conducted similarly to Lorenzetti (2021). The resulting TPWL model is $n_{\text{TPWL}} = 42$ dimensions and requires position and velocity from the the elbows and end effector, resulting in a 30-dimensional observation model. The TPWL OCP is defined with a horizon of $N = 5$, rollout horizon of $N_r = 4$, and discretized in time with $dt = 0.1$ s using a zero-order hold control. The optimal control and state trajectories are interpolated, allowing the feedback controller and state estimator to operate with a control sampling time of $T_s = 0.01$ s.

To obtain a data-driven Koopman model, we sample the configuration space of the robot through a sequence of random control inputs and observe state transitions of the robot's end effector position, where x_{ee}, y_{ee}, and z_{ee} are the x, y, and z coordinates of the end effector. We then compute the model using the toolbox in Bruder et al. (2019a), by transforming the observables into a "lifted" state space. The lifting basis functions consist of all monomials up to order 2 and $d = 1$ time-delay, resulting in a linear model with a lifted state dimension of $n_{\text{Koop}} = 66$. The model's time-discretization and control sampling time are $T_s = dt = 0.1$ s, with horizon of $N = 3$ and rollout horizon of $N_r = 1$.

[1] https://github.com/StanfordASL/soft-robot-control

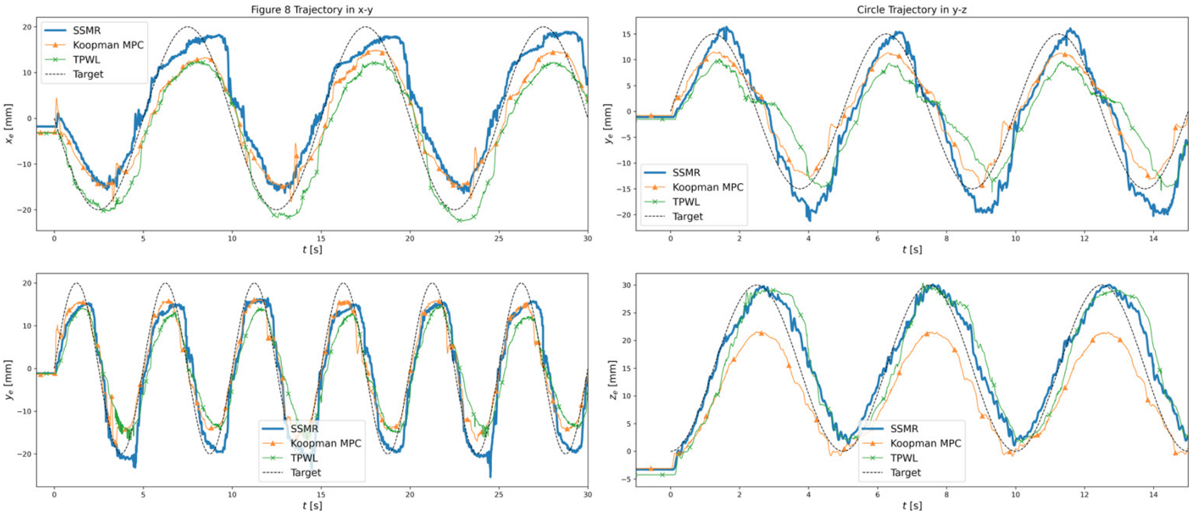

Fig. 2. Experimental results of tracking performance for the Figure 8 (left) and Circle (right) trajectories based on the model and control parameters described in Section 5.2. The TPWL trajectory is shown in green, the Koopman trajectory in orange, and the SSMR in blue. The dotted black line represents the reference trajectory.

To construct the SSMR model, we collect $d = 9$ time-delayed observations of the end effector position, $\mathbf{y} \in \mathbb{R}^{30}$. We obtain this data by displacing the robot along 34 different points in its workspace and observe the decaying trajectory state transitions sampled at $T_s = 10$ ms. This is consistent with the highest frequency mode in the SSM which has a period of roughly 243 ms. After conducting PCA on our training data, we found that the six leading modes captured over 99% of the variance in our dataset.

Since we have access to position and velocity of the end effector, we learn the mappings $\mathbf{w}_z$ and $\mathbf{v}_z$ such that $\mathbf{y} = [x_{\text{ee}}, y_{\text{ee}}, z_{\text{ee}}, \dot{x}_{\text{ee}}, \dot{y}_{\text{ee}}, \dot{z}_{\text{ee}}]$. Due to noise amplification introduced by numerical differentiation, we pass our velocity measurements through a low-pass filter to reduce the noise prior to regression. We fit a cubic order, $n_{\text{SSM}} = 6$ dimensional SSM parametrization and reduced dynamics in (13) using the procedure in Section 4. To fit $\mathbf{B_r}$, we reuse the Figure 8 trajectory and inputs generated by the TPWL model. Our model's time discretization and control sampling time are $T_s = dt = 0.05$ with horizon $N = 6$ and rollout horizon of $N_r = 5$. We remark that the control parameters chosen were tuned for each method to yield the best, real-time performance across all tasks.

5.3 Results

Table 1. A comparison of mean squared tracking error (mm^2) for the Figure 8 and Circle trajectories.

	SSMR (n = 6)	Koopman (n = 66)	TPWL (n = 42)
Figure 8	58.91	57.59	**56.22**
Circle	**29.66**	41.81	64.15

Table 1 reports the mean-squared error tracking performance while Figure 2 depict the experimental results for the quasi-static Figure 8 and Circle trajectories over a single trial. Despite the fact that our SSMR model is only 6-dimensional (compared to 42- and 66-dimensional for the TPWL and Koopman models, respectively), it performs comparably against the other approaches in the Figure 8 trajectory and outperforms them in the Circle trajectory.

Also, while the control terms in the SSMR model were regressed using a Figure 8 trajectory, the model generalizes well to other control tasks. This is due to the fact that we are able to learn the autonomous dynamics faithfully, enabling us to effectively disambiguate the effect of actuation and learn its influence on the reduced dynamics with radically less data (as long as the training trajectories sufficiently explore the actuation space).

A large source of error in our model likely stems from its dependence on velocity in both the model-building phase and the online state estimation phase. Since we obtain velocity through numerical differentiation, the noise introduced by this procedure can degrade our model and corrupt our state estimates during closed-loop operation. Secondly, while our approach is purely data-driven, we still observe the hysteresis phenomenon which plagues the TPWL model but not the data-driven Koopman model (similarly reported in Lorenzetti (2021)). This may be due to the sequential nature in which we disambiguate the effect of controls. While these initial results are promising, we believe that we can achieve even better performance using $d = 1$ time-delays of the end effector position as observables. This would allow us to circumvent the noise introduced by numerical differentiation while implicitly obtaining velocity information.

6. CONCLUSION AND FUTURE WORK

In this work, we provide a rigorous description of our SSMR-based control framework and showcase its real-world applicability for real-time optimal control. We outlined how to learn faithful, low-dimensional dynamics for control on invariant manifolds using pure observation data. We then demonstrated the efficacy of our SSMR-based control scheme on a real-world soft robot, outperforming the current state-of-the-art.

In the future, we plan to extend our approach to state-affine control terms in order to handle a larger class of physicals systems, such as cable- or pneumatically-actuated continuum manipulators. Also, for many physical systems, it may be expensive or difficult to collect experimental data to train the model. Future work will investigate the efficacy of learning SSMR models from high-fidelity FEM simulation to be transferred to the real-world. In this setting, we would employ a hybrid approach where we extract the linear parts from the finite element model and then learn nonlinearities from simulation rollouts.

ACKNOWLEDGEMENTS

The authors would like to thank Riccardo Bonalli for inspiration of the proof of Corollary 10.

REFERENCES

Agrawal, A., Verschueren, R., Diamond, S., and Boyd, S. (2018). A rewriting system for convex optimization problems. *Journal of Control and Decision*, 5(1), 42–60.

Alla, A. and Volkwein, S. (2015). Asymptotic stability of pod based model predictive control for a semilinear parabolic pde. *Advances in Computational Mathematics*, 41(5), 1073–1102.

Alora, J.I., Cenedese, M., Schmerling, E., Haller, G., and Pavone, M. (2022). Data-driven spectral submanifold reduction for nonlinear optimal control of high-dimensional robots (extended version). *arXiv preprint arXiv:2209.05712*.

Altmüller, N. (2014). *Model predictive control for partial differential equations*. Ph.D. thesis.

Axås, J., Cenedese, M., and Haller, G. (2022). Fast data-driven model reduction for nonlinear dynamical systems. *https://arxiv.org/abs/2204.14169arXiv preprint arXiv:2204.14169*.

Bruder, D., Gillespie, B., Remy, C.D., and Vasudevan, R. (2019a). Modeling and control of soft robots using the koopman operator and model predictive control.

Bruder, D., Remy, C.D., and Vasudevan, R. (2019b). Nonlinear system identification of soft robot dynamics using koopman operator theory. In *2019 International Conference on Robotics and Automation (ICRA)*, 6244–6250. IEEE.

Cenedese, M., Axås, J., Bäuerlein, B., Avila, K., and Haller, G. (2022a). Data-driven modeling and prediction of non-linearizable dynamics via spectral submanifolds. *Nature Communications*, 13(1), 872. doi:10.1038/s41467-022-28518-y. URL `https://doi.org/10.1038/s41467-022-28518-y`.

Cenedese, M., Axås, J., Yang, H., Eriten, M., and Haller, G. (2022b). Data-driven nonlinear model reduction to spectral submanifolds in mechanical systems. *Philosophical Transactions of the Royal Society A*, 380(2229), 20210194.

Cranmer, M., Greydanus, S., Hoyer, S., Battaglia, P., Spergel, D., and Ho, S. (2020). Lagrangian neural networks. *arXiv preprint arXiv:2003.04630*.

Dahdah, S. and Forbes, J.R. (2022). System norm regularization methods for koopman operator approximation. *Proceedings of the Royal Society A*, 478(2265), 20220162.

Della Santina, C., Duriez, C., and Rus, D. (2021). Model based control of soft robots: A survey of the state of the art and open challenges. *arXiv preprint arXiv:2110.01358*.

Diamond, S. and Boyd, S. (2016). CVXPY: A Python-embedded modeling language for convex optimization. *Journal of Machine Learning Research*, 17(83), 1–5.

Ghiglieri, J. and Ulbrich, S. (2014). Optimal flow control based on pod and mpc and an application to the cancellation of tollmien–schlichting waves. *Optimization Methods and Software*, 29(5), 1042–1074.

Greydanus, S., Dzamba, M., and Yosinski, J. (2019). Hamiltonian neural networks. *Advances in neural information processing systems*, 32.

Gurobi Optimization, LLC (2022). Gurobi Optimizer Reference Manual. URL `https://www.gurobi.com`.

Haller, G. and Ponsioen, S. (2016). Nonlinear normal modes and spectral submanifolds: existence, uniqueness and use in model reduction. *Nonlinear Dynamics*, 86(3), 1493–1534. doi:10.1007/s11071-016-2974-z. URL `https://doi.org/10.1007/s11071-016-2974-z`.

Haro, A. and de la Llave, R. (2006). A parameterization method for the computation of invariant tori and their whiskers in quasi-periodic maps: Rigorous results. *Journal of Differential Equations*, 228(2), 530–579. doi: https://doi.org/10.1016/j.jde.2005.10.005.

Huang, Y. and Kramer, B. (2020). Balanced reduced-order models for iterative nonlinear control of large-scale systems. *IEEE Control Systems Letters*, 5(5), 1699–1704.

Jain, S. and Haller, G. (2021). How to compute invariant manifolds and their reduced dynamics in high-dimensional finite element models. *Nonlinear Dynamics*. doi:10.1007/s11071-021-06957-4. URL `https://doi.org/10.1007/s11071-021-06957-4`.

Kim, H., Eykholt, R., and Salas, J. (1999). Nonlinear dynamics, delay times, and embedding windows. *Physica D: Nonlinear Phenomena*, 127(1-2), 48–60.

Lorenzetti, J. (2021). *Reduced Order Model Predictive Control of High-Dimensional Systems*. Ph.D. thesis, Stanford University, Dept. of Aeronautics and Astronautics, Stanford, California.

Lorenzetti, J., McClellan, A., Farhat, C., and Pavone, M. (2021). Linear reduced order model predictive control. *IEEE Transactions on Automatic Control*. Submitted.

Mezić, I. (2005). Spectral properties of dynamical systems, model reduction and decompositions. *Nonlinear Dynamics*, 41(1), 309–325.

Samoilenko, A.M. and Teplinsky, Y.V. (2013). *Elements of mathematical theory of evolutionary equations in Banach spaces*, volume 86. World Scientific.

Stellato, B., Banjac, G., Goulart, P., Bemporad, A., and Boyd, S. (2020). OSQP: an operator splitting solver for quadratic programs. *Mathematical Programming Computation*, 12(4), 637–672. doi:10.1007/s12532-020-00179-2. URL `https://doi.org/10.1007/s12532-020-00179-2`.

Thuruthel, T.G., Falotico, E., Renda, F., and Laschi, C. (2018). Model-based reinforcement learning for closed-loop dynamic control of soft robotic manipulators. *IEEE Transactions on Robotics*, 35(1), 124–134.

Tonkens, S., Lorenzetti, J., and Pavone, M. (2021). Soft robot optimal control via reduced order finite element models. *arXiv preprint arXiv:2011.02092*.